Acta Crystallographica Section A
Foundations of Crystallography
ISSN 0108-7673

Received 16 July 2003
Accepted 23 October 2003

Dispersion corrections of the copper *K* edge measured by Fresnel diffraction

Wah-Keat Lee,[a]* Peter Cloetens[b] and Michel Schlenker[c]

[a]Argonne National Laboratory, 9700 S. Cass Avenue, Argonne, IL 60439, USA, [b]European Synchrotron Radiation Facility, BP-220, F-38043 Grenoble, France, and [c]Laboratoire Louis Néel du CNRS, F-38042 Grenoble, France. Correspondence e-mail: wklee@aps.anl.gov

Dispersion corrections to the atomic scattering factors for the copper K edge have been measured by a new technique, Fresnel diffraction. Fresnel diffraction fringes were measured at several sample–detector distances as a function of energy across the copper *K*-absorption edge. The dispersion corrections were obtained from optimizing a least-squares fit of Fresnel fringe simulations to the measured data.

1. Introduction

X-ray dispersion corrections to the atomic scattering factors, sometimes called Hönl corrections, or anomalous-scattering terms are indispensable for any quantitative X-ray diffraction analysis. Atomic X-ray scattering factors are usually written as

$$f(\mathbf{q}, E) = f_0(\mathbf{q}) + f'(\mathbf{q}, E) + if''(\mathbf{q}, E), \tag{1}$$

where f' and f'' are the dispersion corrections. Atomic scattering factors are a measure of the scattering amplitude of the atom with respect to a single free electron. In general, the scattering factor depends on both the energy of the incident radiation, E, and the scattering vector, $\mathbf{q} = \mathbf{k}_{\rm out} - \mathbf{k}_{\rm in}$, where $\mathbf{k}_{\rm in}$ and $\mathbf{k}_{\rm out}$ are the incident and scattered wavevectors, respectively. $|q| = 4\pi \sin\theta/\lambda$, where 2θ is the scattering angle and λ is the wavelength. In the non-relativistic regime, for $q = 0$, f_0 is the number of electrons in the atom, Z. f' and f'' depend on the atomic absorption frequencies and are related to one another by the Kramers–Kronig relation:

$$\begin{aligned} f'(\omega) &= \frac{2}{\pi} P \int_0^\infty \frac{\omega' f''(\omega')}{\omega'^2 - \omega^2}\, {\rm d}\omega' \\ f''(\omega) &= \frac{-2\omega}{\pi} P \int_0^\infty \frac{f'(\omega')}{\omega'^2 - \omega^2}\, {\rm d}\omega', \end{aligned} \tag{2}$$

where P denotes the Cauchy principal value of the integral and $E = \hbar\omega$.

The atomic form factors are related to the material's index of refraction, $n = 1 - \delta + i\beta$. For a single element, this is given by

$$\delta = \frac{r_e \lambda^2 N_A \rho (f_0 + f')}{2\pi A}, \quad \beta = \frac{r_e \lambda^2 N_A \rho f''}{2\pi A}, \tag{3}$$

where r_e is the classical electron radius, ρ is the mass density, N_A is the Avagadro number and A is the atomic mass.

The imaginary part of the index of refraction is related to the material's linear absorption coefficient:

$$\mu = 4\pi\beta/\lambda. \tag{4}$$

The real part of the index of refraction is related to the phase velocity of the X-rays. Therefore, techniques that are sensitive to the material's index of refraction can be used to measure dispersion corrections.

Since the electrons in the atom are bound and not free, it can be expected that f_0 should be slightly less than Z. Using relativistic multipole calculations, it can be shown (Smith, 1987) that the reduction in scattering power, expressed in electrons, is $-E_{\rm tot}/mc^2$, where $E_{\rm tot}$ is the total ground-state binding energy of all the electrons in the atom. Thus, even in the limit of frequencies much higher than the absorption frequencies, the $q = 0$ scattering factor is slightly less than Z. Although this relativistic correction term is independent of the X-ray energy (non-dispersive), experimentalists usually incorporate it into their stated values of f', defining the forward-scattering factor as: $f = Z + f' + if''$ and referring to f' as the real part of the dispersion correction. We follow the same convention in this paper. In our case, for copper, the relativistic correction is 0.085 electron (Kissel & Pratt, 1990) and is small compared to our measurement errors.

Dispersion correction measurements can be divided into two types: (i) measurements at finite q, and (ii) measurements in the forward direction, $q = 0$. The techniques that measure the dispersion corrections at finite q include absolute diffracted intensity (Freund, 1975; Suortti *et al.*, 1985) and *Pendellösung* (Takama & Sato, 1982) measurements. They rely on the fact that the scattered intensity and the *Pendellösung* fringes depend on the structure factor, which, in turn, depends on the atomic scattering factors. One result from these measurements is that no definite q dependence has been found in the dispersion corrections (Creagh, 1999). This is consistent with the fact that the largest contribution to the dispersion correction is from the *K*-shell electrons, which are close to the nucleus and spherically symmetric. In the $q = 0$ forward direction, dispersion corrections have been measured by interferometry (Creagh & Hart, 1970; Cusatis & Hart, 1977;

Hart & Siddons, 1981; Bonse *et al.*, 1982, Siddons & Hart, 1983; Bonse *et al.*, 1983*a*,*b*; Bonse & Hartmann-Lotsch, 1984; Begum *et al.*, 1986; Bonse *et al.*, 1989), reflectivity (Stanglmeier *et al.*, 1992), angular deviations from prisms (Deutsch & Hart, 1984; Fontaine *et al.*, 1985) and absorption (Dreier *et al.*, 1984; Hoyt *et al.*, 1984). Review articles have been written by Lengeler (1994) and Creagh (1999).

In this paper, we describe a new method of measuring the $q = 0$ dispersion corrections, namely by Fresnel diffraction. The wave transmitted through a sample is sensitive to the sample's index of refraction. In particular, the phase of the transmitted wavefront will be affected by the real part of the index of refraction, while the amplitude will be affected by the imaginary part. For a coherent beam, the various components of this distorted and attenuated wavefront will interfere and, after propagation over a finite distance, produce Fresnel fringes. Given a geometrically simple sample, we show that it is possible to retrieve the material's index of refraction from its Fresnel diffraction patterns. As in interferometry, this technique measures both the real and imaginary parts of the atomic form factors simultaneously.

2. Theory

The interaction of X-rays with matter is very weak and, away from Bragg conditions, the diffraction angles are very small ($\sim 10^{-6}$). Thus, provided the sample is not too thick, we can neglect the lateral shift suffered by the X-ray beam in the sample. Assuming the X-rays travel in the z direction, the transmission function of a one-dimensional object can be written as:

$$T(x) = A(x)\exp[i\varphi(x)], \tag{5}$$

where the amplitude $A(x)$ is related to the linear absorption coefficient μ:

$$\begin{aligned} A(x) &= \exp[-B(x)] \\ B(x) &= (2\pi/\lambda)\int \beta(x, z)\,\mathrm{d}z = \int [\mu(x, z)/2]\,\mathrm{d}z, \end{aligned} \tag{6}$$

and the phase $\varphi(x)$ is given by

$$\varphi(x) = (2\pi/\lambda)\int [1 - \delta(x, z)]\,\mathrm{d}z = \varphi_0 - (2\pi/\lambda)\int \delta(x, z)\,\mathrm{d}z, \tag{7}$$

where φ_0 is a constant that represents the accumulated phase in the absence of the sample and can be neglected. B and φ are therefore directly related to f'' and f', respectively. The transmitted wave immediately after the sample can be written as:

$$\psi_0(x) = \psi_{\mathrm{inc}}(x)T(x), \tag{8}$$

where ψ_{inc} is the incident wave and $T(x)$ is the transmission function characterizing the specimen. At a distance L from the sample, the wave can be calculated using the Fresnel approximation to the Huygens–Kirchhoff integral (Born & Wolf, 1999):

$$\psi_L(x) = \frac{\exp(ikL)}{(i\lambda L)^{1/2}}\int \psi_0(x')\exp[ik(x - x')^2/2L]\,\mathrm{d}x', \tag{9}$$

where $k = 2\pi/\lambda$ is the vacuum wavenumber. Thus, given the material's index of refraction and the sample geometry, one can calculate the diffraction pattern at a distance L from the sample. In this experiment, we use a simple object, namely a copper fiber, to measure the dispersion corrections over the K edge.

3. Experimental set-up

The experiments were performed at the ID19 beamline at the European Synchrotron Radiation Facility (ESRF). The experimental station on this beamline, which is primarily used for X-ray imaging, is 145 m from the source and, thus, the beam has excellent lateral coherence. At ID19, the source sizes are 25 µm in the vertical direction and 125 µm in the horizontal direction (FWHM). At 145 m from the source, the lateral coherence lengths are 127 µm vertically and 25 µm horizontally for 9 keV X-rays. With a high-quality X-ray detector, it is possible to resolve the fine details of fringes due to Fresnel diffraction. The detection system consists of an X-ray scintillator (europium-doped $Lu_3Al_5O_{12}$ single crystal), a 20× microscope objective with 0.4 numerical aperture, and a cooled CCD camera with 2048 × 2048 pixels and a dynamic range of 14 bits. The demagnified CCD pixel size is 0.69 µm, and the resolution of the detection system is about 1.5 µm. Diffraction patterns from a 10 µm-diameter copper fiber (10% tolerance, purchased from Goodfellow, Great Britain) were recorded at ten different sample–detector distances (9.4–886.4 mm). The copper fiber was held with its axis approximately horizontal to take advantage of the higher beam coherence in the vertical direction. Images with and without the fiber, together with images without the X-ray beam ('dark field') were recorded. A 'flat-fielded' image, $I^{\mathrm{meas}}(x, y)$, is obtained by:

$$I^{\mathrm{meas}}(x, y) = [I(\mathrm{sample}) - I(\mathrm{dark})]/[I(\mathrm{nosample}) - I(\mathrm{dark})]. \tag{10}$$

Figs. 1(*a*) and 1(*b*) show a section of the flat-field-corrected fringe patterns for 8975 eV, taken at 9.4 and 886.4 mm from the sample, respectively. The sheer number of diffraction fringes testifies to the high degree of beam coherence and the excellent detector system. Clean sections of the Fresnel fringe patterns, free of spurious features due to dust or scratches coming from the monochromator crystals or vacuum windows upstream, or singularities due to the scintillator crystal, were selected by inspection and averaged over 200 pixels in the dimension parallel to the fiber axis for better statistics. The averaged data are therefore represented as $I(x)^{\mathrm{meas}}$ with a corresponding standard deviation $\sigma(x)^{\mathrm{meas}}$. Each fringe pattern consists of 414 data points. The measurements were performed for 20 different energies across the Cu K edge, from 8975 to 9045 eV. The energy was selected by a silicon double-crystal monochromator operating in the vertical plane for the 111 reflection in Bragg geometry.

4. Data analysis

In theory, it should be possible to obtain the index of refraction directly by phase reconstruction of the fringe patterns (Cloetens *et al.*, 1997). However, owing to the relatively large phase jumps involved, this approach was not successful. Instead, we simulated the diffraction patterns and performed a least-squares minimization on the difference between the measured and simulated data.

The simulation method is described by Cloetens (1999) and only the essential aspects will be mentioned here. For the incident wave, we used the parabolic approximation to a spherical wave. At a distance L downstream of the sample, the calculated detected intensity is:

$$I(x)^{\rm calc} = |\psi_L(x)|^2 * R_{\rm eff}(x), \tag{11}$$

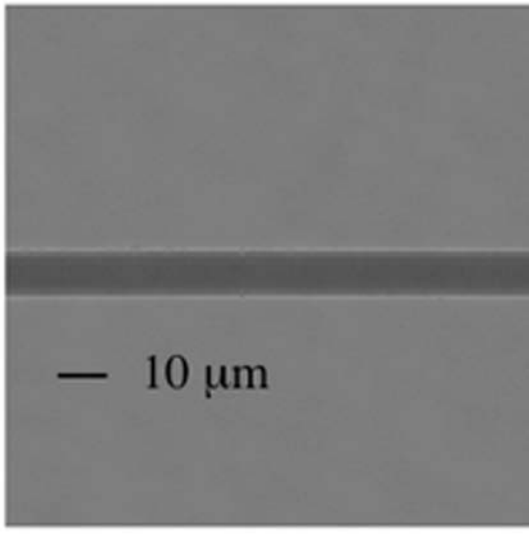

(*a*)

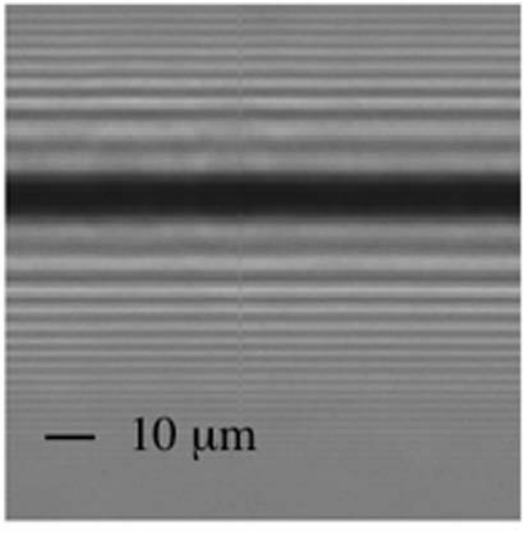

(*b*)

Figure 1
Flat-fielded image of copper fiber, E = 8975 eV. (*a*) L = 9.4 mm and (*b*) L = 886.4 mm. The diameter of the fiber is approximately 10 μm. The demagnified CCD pixel size is 0.69 μm.

where $R_{\rm eff}$ is an effective resolution function that includes the detector resolution and the beam degree of coherence, and * denotes convolution. In practice, the convolutions in (9) and (11) are not calculated in direct space but rather *via* an equivalent multiplication in reciprocal space. $I^{\rm calc}$ depends on several parameters: fiber radius (r), wavelength (λ), distance (L), f' (*via* the minimum value of the phase at the centre of the fiber, $\varphi_{\rm max} = -4\pi r\delta/\lambda$), f'' (*via* the maximum attenuation, $B_{\rm max} = 4\pi r\beta/\lambda$) and $R_{\rm eff}$. For each energy, ten measurements at different distances L were made by translating the detector. Owing to the imperfections of the detector translation stage, the measurements taken at different sample–detector distances L were misaligned relative to one another. The gross misalignments were handled by relative translations of the data so that the centers of the fringe patterns were within one pixel of one another. The finer misalignment was handled by introducing an additional parameter, *xoffset*, for each data set in the simulation.

The data-fitting procedure involves minimization of the chi-square sum:

$$\chi^2 = \sum \left[\frac{I^{\rm calc} - I^{\rm meas}}{\sigma^{\rm meas}}\right]^2. \tag{12}$$

In order to avoid being trapped in a local minimum, the minimization was done in stages and iteratively. Briefly, for each energy, the fitting procedure was performed as follows: The first fits were done using r, $B_{\rm max}$, $\varphi_{\rm max}$ and an average *xoffset* as the fit parameters. In order to compensate for some fluctuations in the average intensity, the measured data were normalized such that the intensity in the wings of the data (where there are no fringes) match that of this initial fit. For the fitting procedure, the *inital* values used for all the energies are: $\varphi_{\rm max} = -8.0$, $B_{\rm max} = 0.5$, $r = 5$ μm (manufacturer specification), λ from the beamline monochromator calibration, L was measured and $R_{\rm eff}$ was measured several months prior to the experiment at an X-ray energy of 20 keV. Next, using these results, fits were done to obtain the optimum individual *xoffset* parameter for each fringe pattern. The final fits involve only two fitting parameters, $\varphi_{\rm max}$ and $B_{\rm max}$. This was done for different values of r so that the optimum value of r could be determined from the chi-square when summed over *all* the energies. A final value of r = 5.3 μm was obtained. The optimized values of $\varphi_{\rm max}$ and $B_{\rm max}$ were then used to optimize the resolution function $R_{\rm eff}$, described as a sum of four Gaussians, and this process was performed iteratively. When minimizing the chi-square over *all* the energies, data from energies 9001 and 9003 eV were omitted. The images from these two energies were of poor quality owing to the emergence of additional structures on the scintillator. The reason for this is as yet unknown, but we suspect that it has to do with Bragg diffraction within the scintillator at those particular energies. Fig. 2 shows a typical fit to the data. The reduced chi-square (χ^2_ν) value for the entire data set, summed over all the energies, is 0.8. Individual reduced chi-square values for each fringe pattern (except 9001 and 9003 eV) vary from 0.4 to 2.1. After the optimization was done, we noticed that the f' and f''

results of our measurements appear to be shifted to the low-energy side by about 5 eV relative to the literature. This suggests that there was an error in the calibration of the beamline monochromator, which was performed by the Bond method (Bond, 1960). The optimization process was then repeated using the corrected (beamline calibration energy +5 eV) energies. The beam energies stated in this paper are the corrected values.

It is important to estimate the errors on the measured dispersion corrections. Chi-square sums around the best values of f' and f'' were calculated. The error in the fitted parameters due to the chi-square minimization procedure can be estimated graphically or analytically by (Bevington & Robinson, 1992)

$$(\Delta f'_{\rm fit})^2 = 2\left(\frac{\partial^2 \chi^2}{\partial f'^2}\right)^{-1}, \qquad (13)$$

with a similar expression for f''. Another source of error comes from uncertainty in the optimized values of r, λ, L, $R_{\rm eff}$ and *xoffset*, which were held constant in the final fit of $\varphi_{\rm max}$ and $B_{\rm max}$. Errors in the values of the dispersion corrections from uncertainty in these variables were approximated by:

$$(\Delta f'_{\rm par})^2 = \left(\frac{\partial f'}{\partial r}\Delta r\right)^2 + \left(\frac{\partial f'}{\partial \lambda}\Delta\lambda\right)^2 + \left(\frac{\partial f'}{\partial L}\Delta L\right)^2 + \left(\frac{\partial f'}{\partial R_{\rm eff}}\Delta R_{\rm eff}\right)^2 + \left(\frac{\partial f'}{\partial xoffset}\Delta xoffset\right)^2, \qquad (14)$$

with a similar expression for f''. $\Delta\lambda$ was estimated to be 0.00046 Å (3 eV in energy) from the bandwidth of the monochromatic beam and the accuracy by which we can determine the absorption edge from the data. ΔL was estimated to be 0.5 mm from the measurements of the sample-to-detector distance. The contribution to the error from the effective resolution function $R_{\rm eff}$ was obtained from the difference between the dispersion values resulting from an optimized $R_{\rm eff}$ and from the original value of $R_{\rm eff}$ that was measured several months prior to this experiment. Note that $R_{\rm eff}$ is a function (sum of four Gaussians), and the notation $\Delta R_{\rm eff}$ in (14) denotes the change in the parameters (amplitudes and widths of the Gaussians) of the function but not the function itself. The contribution from the *xoffset* parameter was obtained from the difference between the dispersion values resulting from an optimized *xoffset* and from not using them at all (by setting *xoffset* = 0). We estimate Δr from the variance of the optimum radius obtained from the initial fits at different energies where r was a fit parameter instead of a constant. From the fits, $r = 5.30\pm0.06$ µm. After the experiment, the diameter of the fiber was measured with a scanning electron microscope (SEM). The SEM measurements confirm our best-fit results for the radius and also confirm that the

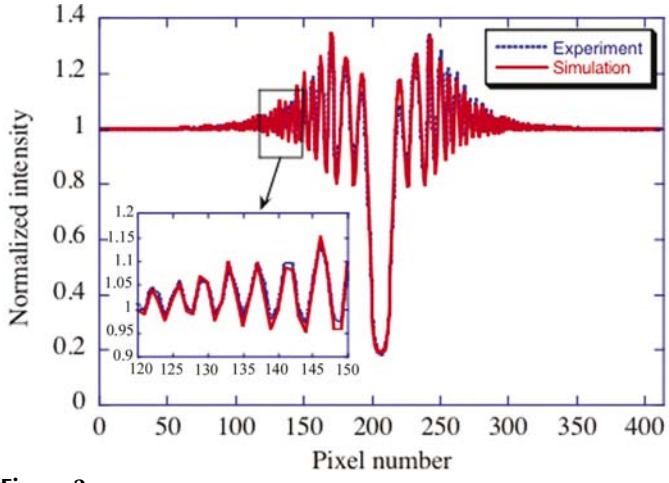

Figure 2
A typical example of the fit between the experimental data and the simulation. This is for E = 8975 eV and L = 886.4 mm.

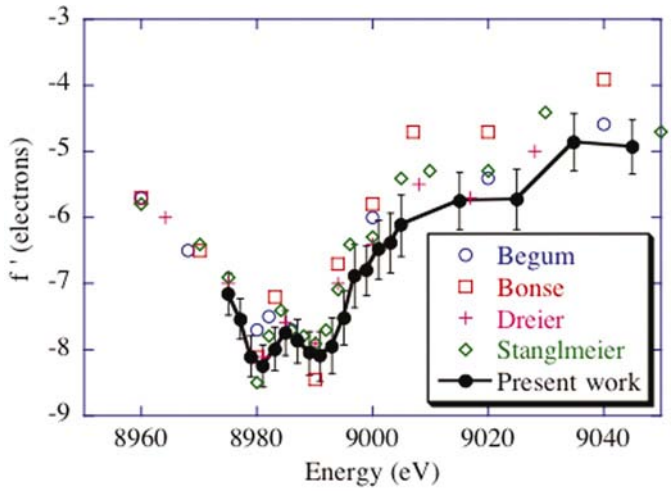

Figure 3
Plot of f' *versus* energy for the Cu K edge. The data from Begum *et al.* (1986) was by interferometry, Bonse *et al.* (1982) and Dreier *et al.* (1984) by Kramers–Kronig transformation of absorption data, and Stanglmeier *et al.* (1992) was by reflection. The error bars correspond to one standard deviation.

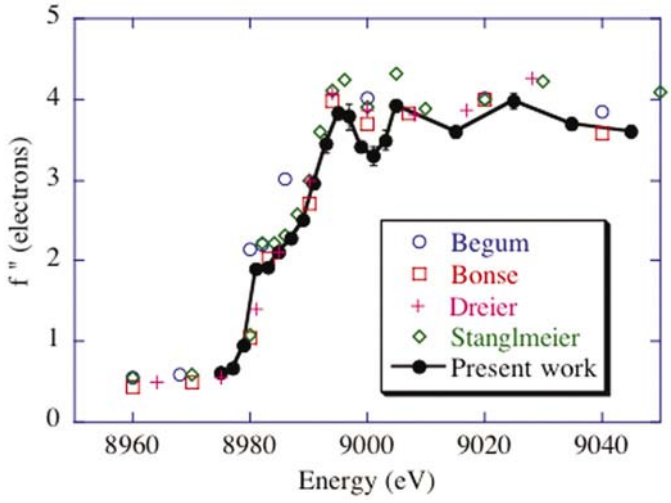

Figure 4
Plot of f'' *versus* energy for the Cu K edge. The data from Begum *et al.* (1986) was by interferometry, Bonse *et al.* (1982) and Dreier *et al.* (1984) by absorption, and Stanglmeier *et al.* (1992) was by reflection. The error bars correspond to one standard deviation.

Table 1
Average contributions to the errors (one standard deviation values) in the dispersion corrections from the optimization procedure; individual errors for each energy differ slightly.

Parameter	$\Delta f'$ (electrons)	$\Delta f''$ (electrons)
L	0.039	0.007
$R_{\rm eff}$	0.108	0.035
λ	0.026	0.002
xoffset	0.035	0.029
r	0.326	0.050
Fitting process [equation (13)]	0.036	0.003
Total	0.350	0.068

sample was indeed cylindrical. A summary of the average errors from each of these parameters is listed in Table 1.

A comparison of our data with those from interferometry (Begum *et al.*, 1986), absorption (Bonse *et al.*, 1982; Dreier *et al.*, 1984) and reflectivity (Stanglmeier *et al.*, 1992) are shown in Figs. 3 and 4. (We only show a few of the numerous experimental results from the literature to avoid overcrowding the plots.) The wiggles in the data are due to solid-state effects, such as EXAFS. It can be seen that the agreement is quite good. For the first minimum of f' (at ~8980 eV), surveys of previous experimental results give an unweighted average value of -8.54 ± 0.62 electrons (Creagh, 1999) and a weighted average value of -8.4 ± 0.2 electrons (Lengeler, 1994). Our measurements give -8.24 ± 0.30 electrons, which is within the range of the surveyed results.

5. Conclusions

This paper presents a new technique for measuring dispersion corrections to the X-ray atomic scattering factors, namely by analysis of the Fresnel diffraction patterns. The main advantages of this technique are its simplicity and robustness. There are no constraints on the sample environment, aside from the necessity of it being a simple geometrical object. Thus, it is possible to make these measurements under different sample environments, for example, as a function of temperature or magnetic fields and/or under different incident X-ray polarization. Note that sample chamber windows are not a concern in this technique. Although we used a fiber in this study, this technique should be equally applicable using the edge of a foil or the edge of a thin layer of material deposited onto a plate. Thus, the range of materials is not restricted to those that can be made into thin fibers. With interferometry, one is usually restricted in the space around the sample since interferometers tend to be fairly small (~2–5 cm) devices. Their high sensitivity requires that the environment be extremely stable and without any thermal drifts. For example, positioning electromagnets around the sample would be a difficult challenge. Furthermore, it would not be possible to make measurements with circularly polarized X-rays because the beam polarization would change as it travels through the blades of the interferometer. With reflectivity, one is restricted to materials that can be made into an X-ray mirror (*via* deposition to a substrate or direct polishing). For coated mirrors, it would be difficult to make these measurements under different environment conditions, such as under strain or high temperature where there would be the risk of damage to the coating. The disadvantage of our technique is that, for good results, the measured Fresnel patterns should contain a large number of fringes. This puts a requirement on the thickness of the sample and the resolution of the detection system, which becomes harder to achieve at higher energies. The average estimated errors in our measurement, ±0.35 electron for f' and ±0.07 electron for f'', are comparable to those stated in the literature. The largest source of error comes from uncertainty in the thickness (or diameter) of the sample. Aside from the determination of dispersion corrections, another possible application of this quantitative fringe analysis technique is element- and oxidation-state-sensitive phase contrast imaging. Absorption edges and the dispersion corrections are unique to each element and are influenced by the element's oxidation state. By applying similar analysis in combination with phase tomography (Cloetens, 1999), it should be possible to map the spatial distribution of different elements and different oxidation states of the same element within a complex sample. This should provide much better sensitivity compared to absorption-based imaging techniques.

WKL was supported by the US Department of Energy, Office of Science, contract No. W-31-109-Eng-38. This work was performed while WKL was a visiting scientist at the ESRF. We thank Annick Liénard of the Laboratoire Louis Néel du CNRS for the SEM measurements.

References

Begum, R., Hart, M., Lea, K. R. & Siddons, D. P. (1986). *Acta Cryst.* A**42**, 456–464.
Bevington, P. R. & Robinson, D. K. (1992). *Data Reduction and Error Analysis for the Physical Sciences*, 2nd ed. New York: WCB McGraw-Hill.
Bond, W. L. (1960). *Acta Cryst.* **13**, 814.
Bonse, U. & Hartmann-Lotsch, I. (1984). *Nucl. Instrum. Methods*, **222**, 185–188.
Bonse, U., Hartmann-Lotsch, I. & Lotsch, H. (1983*a*). *EXAFS and Near Edge Structure*, edited by A. Bianconi, L. Incoccia & S. Stipcich, pp. 376–377. Berlin: Springer.
Bonse, U., Hartmann-Lotsch, I. & Lotsch, H. (1983*b*). *Nucl. Instrum. Methods*, **208**, 603–604.
Bonse, U., Hartmann-Lotsch, I., Lotsch, H. & Olthoff-Munter, K. (1982). *Z. Phys. B*, **47**, 297–299.
Bonse, U., Lotsch, H. & Henning, A. (1989). *J. X-ray Sci. Techn.* **1**, 107–120.
Born, M. & Wolf, E. (1999). *Principles of Optics*, 7th ed. Cambridge University Press.
Cloetens, P. (1999). PhD thesis, Vrije Universiteit Brussel, Belgium.
Cloetens, P., Guigay, J.-P., De Martino, C., Salome, M., Schlenker, M. & Van Dyck, D. (1997). *SPIE*, **3154**, 72–82.
Creagh, D. C. (1999). *X-ray Dispersion Corrections. International Tables for Crystallography*, Vol. C, edited by A. J. C. Wilson & E. Prince, Section 4.2.6, p. 242. Dordrecht: Kluwer.
Creagh, D. C. & Hart, M. (1970). *Phys. Status Solidi*, **37**, 753–758.
Cusatis, C. & Hart, M. (1977). *Proc. R. Soc. London Ser. A*, **354**, 291–302.

Deutsch M. & Hart, M. (1984). *Phys. Rev. B*, **30**, 640–642.
Dreier, P., Rabe, P., Malzfeldt, W. & Niemann, W. (1984). *J. Phys. C*, **17**, 3123–3136.
Fontaine, A., Warburton, W. K. & Ludwig, K. F. (1985). *Phys. Rev. B*, **31**, 3599–3605.
Freund, A. (1975). *Anomalous Scattering*, edited by S. Ramaseshan & S. C. Abrahams, pp. 69–84. Copenhagen: Munksgaard.
Hart, M. & Siddons, D. P. (1981). *Proc. R. Soc. London Ser. A*, **376**, 465–482.
Hoyt, J. J., de Fontaine, D. & Warburton, W. K. (1984). *J. Appl. Cryst.* **17**, 344–351.
Kissel, L. & Pratt, R. H. (1990). *Acta Cryst.* A**46**, 170–175.
Lengeler, B. (1994). *Resonant Anomalous X-ray Scattering: Theory and Applications*, edited by G. Materlik, C. J. Sparks & K. Fischer, pp. 35–60. Amsterdam: Elsevier.
Siddons, D. P. & Hart, M. (1983). *EXAFS and Near Edge Structure*, edited by A. Bianconi, L. Incoccia & S. Stipcich, pp. 373–375. Berlin: Springer.
Smith, D. Y. (1987). *Phys. Rev. A*, **35**, 3381–3387.
Stanglmeier, F., Lengeler, B., Weber, W., Gobel, H. & Schuster, M. (1992). *Acta Cryst.* A**48**, 626–639.
Suortti, P., Hastings, J. B. & Cox. D. E. (1985). *Acta Cryst.* A**41**, 417–420.
Takama, T. & Sato, S. (1982). *Philos. Mag.* **45**, 615–626.